Excited State, Charge Transfer, and Spin Dynamics in DNA Hairpin Conjugates with Perylenediimide Hairpin Linkers[†]

Raanan Carmieli, Tarek A. Zeidan, Richard F. Kelley, Qixi Mi, Frederick D. Lewis,* and Michael R. Wasielewski*

Department of Chemistry and Argonne-Northwestern Solar Energy Research (ANSER) Center, Northwestern University, Evanston, Illinois 60208-3113

Received: January 9, 2009

A series of short DNA hairpins (**nG**) using perylene-3,4:9,10-bis(dicarboximide) (PDI) as the hairpin linker was synthesized in which the distance between the PDI and a guanine−cytosine (G-C) base pair is systematically varied by changing the number $(n - 1)$ of adenine−thymine (A-T) base pairs between them. Due to the relatively large hydrophobic surface of PDI, the **nG** hairpins dimerize in buffer solutions. The photophysics and photochemistry of these hairpins were investigated using femtosecond transient absorption and time-resolved electron paramagnetic resonance (TREPR) spectroscopy. Photoexcitation of the self-assembled PDI dimer within each **nG** hairpin results in subpicosecond formation of its lower exciton state ($^{1*}PDI_2$) followed by formation of an excimer-like state ($^{1*X}PDI_2$) with $\tau = 10-28$ ps. Both of these states are lower in energy than $^{1*}PDI$, so that neither can oxidize A, C, and T. Electron transfer from G to $^{1*}PDI_2$ is faster than formation of $^{1*X}PDI_2$ only for **1G**. Electron transfer from G to $^{1*X}PDI_2$ for **2G−8G**, occurs by the superexchange mechanism and, thus, becomes exponentially less efficient as the G-PDI$_2$ distance increases. Nevertheless, TREPR studies show that photoexcitation of **2G** and **4G** produce spin-correlated radical ion pairs having electron spin polarization patterns indicating that a low yield of charge separation proceeds from $^{1*X}PDI_2$ by the radical pair intersystem crossing (RP-ISC) mechanism to initially yield a singlet radical ion pair. The strong spin-polarization of the radical ion pairs makes it possible to observe them, even though their concentration is low. As expected, the hairpin lacking G (**0G**) and that having the longest G-PDI$_2$ distance (**8G**) display no TREPR radical ion pair signals. Hairpins **0G**, **2G**, **4G**, and **8G** all exhibit triplet EPR spectra at 85 K. Simulations of the spectra show that $^{3*}PDI$ is produced mainly by a spin−orbit-induced intersystem crossing mechanism, while the spectra of **2G** and **4G** have 5% and 21% contributions, respectively, from $^{3*}PDI$ produced by charge recombination of radical ion pairs that originate from RP-ISC. These low percentages of RP-ISC derived $^{3*}PDI$ result mainly from the low yield of radical ion pairs in **2G** and **4G**.

Introduction

Understanding charge transport through DNA has become a major interest in the past decade. Charge transport in DNA is important not only in biology, where photochemical oxidation of the DNA can result in DNA damage, but also in the development of DNA-based nanotechnologies. The hydrogen-bonded, π-stacked base pairs in DNA provide a potential pathway for charge transport, which has led to the proposal that DNA can serve as a molecular wire.[1−4] Studies of charge transport in DNA have used a variety of experimental techniques including strand cleavage studies,[5,6] fluorescence quenching,[7−10] nanosecond and femtosecond transient absorption spectroscopy,[11−14] line shape analyses of steady-state (continuous wave, CW) EPR spectra,[15−18] and, more recently, time-resolved EPR (TREPR) spectroscopy.[19,20]

Here, we use TREPR in addition to femtosecond transient optical spectroscopy to study charge transport in DNA hairpin dimers. TREPR is a well-established method for measuring radical pair (RP) and triplet-state properties in donor−acceptor systems.[21−23] The experiment involves the application of a laser pulse to the sample followed by measurement of the transient EPR spectrum using either CW microwaves or a series of microwave pulses for detection. While transient optical spectroscopy has a clear advantage in providing time resolution down to the femtosecond regime, the transient spectra of the excited states, oxidized donor, and reduced acceptor frequently overlap, thereby complicating the kinetic analysis. In contrast, TREPR suffers from a comparatively low time resolution of about 10 ns but has the advantage of directly yielding the electronic coupling between the donor and acceptor radical ions as reflected in their spin−spin exchange interaction, $2J$, as well as providing structural information, such as the distance between the two radicals as determined from their spin−spin dipolar interaction, D. This results from the sensitivity of TREPR to weak interactions that cannot be resolved by optical techniques for large molecules. The combination of optical spectroscopy and TREPR enables us to study charge transport in DNA over a broad range of times scales that yield complementary information about the system.

We recently reported the results of an investigation of the dynamics and mechanism of photoinduced electron transfer in a series of synthetic DNA hairpins in which the perylene-3,4:9,10-bis(dicarboximide) (PDI) chromophore is incorporated into an oligonucleotide as a base pair surrogate.[20] The photoinduced charge transfer and spin dynamics of these hairpins were studied using femtosecond transient absorption and TREPR spectroscopy. PDI is a sufficiently powerful photooxidant to quantita-
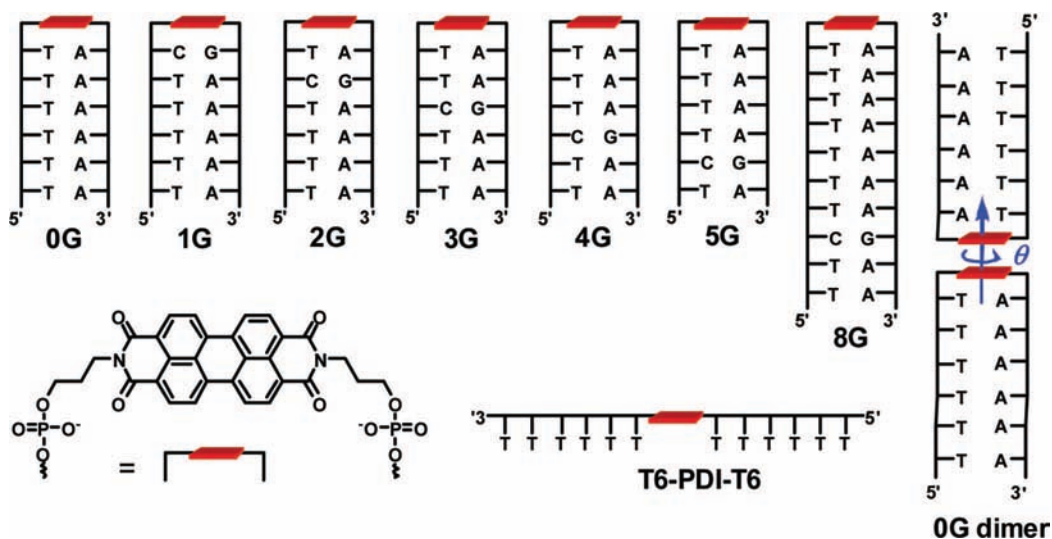
Figure 1. Structure of the PDI chromophore and the PDI-DNA conjugates.

tively inject holes into adjacent adenine (A) and guanine (G) nucleobases. Charge transfer dynamics observed following hole injection from PDI into the A-tract of the DNA hairpins are consistent with formation of a polaron involving an estimated three to four A bases. Trapping of the $(A_{3-4})^{+\bullet}$ polaron by a G base at the opposite end of the A-tract from PDI is only competitive with charge recombination of the polaron and PDI$^{-\bullet}$ at short G-PDI distances. In a hairpin having three A-T base pairs between PDI and G, the RP that results from trapping the hole by G is spin-correlated and displays TREPR spectra at 295 and 85 K consistent with its formation from ^{1*}PDI by the radical pair intersystem crossing (RP-ISC) mechanism. Charge recombination is spin-selective and produces ^{3*}PDI, which at 85 K exhibits a spin-polarized TREPR spectrum that is diagnostic for its origin from the spin-correlated RP. Interestingly, in a hairpin having no G bases, TREPR spectra at 85 K reveal a spin-correlated radical pair with a dipolar interaction identical to that of the hairpin having three A-T base pairs between PDI and G implying that the A-base in the fourth A-T base pair away from the PDI chromophore serves as a hole trap. Our data suggest that hole injection and transport in these hairpins is completely dominated by polaron generation and movement to a trap site rather than by superexchange. On the other hand, the barrier for charge injection from G$^{+\bullet}$ back onto the A-T base pairs is strongly activated, so that charge recombination from G (or even A trap sites at 85 K) most likely proceeds by a superexchange mechanism.

We now report on excited-state dynamics and photoinduced charge transfer involving DNA hairpins in which the PDI chromophore itself serves as the hairpin linker. A series of seven hairpins were investigated in which the PDI linker and a G within a G-C base pair, which serves as a hole trap, are separated systematically by different numbers of A-T base pairs (Figure 1). These systems form structures in which the exposed side of the PDI π system within one hairpin dimerizes with the PDI of a second hairpin in buffer solution as a result of the large PDI hydrophobic surface.[24] This dimerization motif is illustrated for **0G** in Figure 1, where θ is defined as the torsional angle between the vectors along the N−N axes of the two cofacial PDI molecules. In addition, the single-stranded T_6-PDI-T_6 conjugate is included as a reference molecule in which the PDI remains monomeric.

Experimental Section

Synthesis and Characterization. The PDI hairpins **nG** as well as T_6-**PDI**-T_6 were prepared according to the procedure of Letsinger and Wu[25] and modified by Rahe et al.[26] to incorporate the PDI linker. The PDI conjugates were purified by HPLC and characterized by MALDI-TOF mass spectrometry (Table S1 in Supporting Information). UV−vis absorption measurements were made on a Shimadzu spectrometer (UV1601). All optical measurements were performed at room temperature except where noted. Steady-state emission was measured on a PTI QuantaMaster 1 single photon counting spectrofluorimeter in a right angle configuration.

Transient Absorption Spectroscopy. Femtosecond measurements were made using a Ti:sapphire laser system.[27] The instrument response function (IRF) for the pump−probe experiments was 180 fs. Typically, 5 s of averaging was used to obtain the transient spectrum at a given delay time. Solutions of conjugates in 10 mM phosphate buffer, 100 mM NaCl, pH 7.4, were prepared in cuvettes having a 2 mm path length and were irradiated with 505 nm, 130 fs, 0.1−1.0 μJ pulses focused to a 200 μm diameter spot. The optical density at λ_{ex} was between 0.2 and 0.4. Laser scatter at 505 nm was subtracted from the transient spectra. The three-dimensional data sets of ΔA vs time (0−6 ns) and wavelength (440−800 nm) were subjected to singular value decomposition and global fitting to obtain the kinetic time constants and their associated spectra using Surface Xplorer software.[28]

Fluorescence Lifetimes. Fluorescence lifetime measurements were performed using a frequency-doubled, cavity-dumped Ti: sapphire laser as the excitation source and a Hamamatsu C4780 ps fluorescence lifetime measurement system as described previously.[23] The energy of the 400 nm, 25 fs pulses was attenuated to approximately 1.0 nJ/pulse for all fluorescence lifetime experiments. The total IRF of the streak camera system was 20 ps. The samples were prepared in 1 cm path length quartz cuvettes, and time-resolved data were collected for each sample at the same concentrations as the steady-state data. All fluorescence data were acquired in single photon counting mode using Hamamatsu HPD-TA software. The data were fit using the Hamamatsu fitting module and deconvoluted using the laser pulse profile.

EPR Spectroscopy. DNA samples for EPR measurements were prepared in the following way: 0.8 mM of DNA sample

Charge Transport through DNA

J. Phys. Chem. A, Vol. 113, No. 16, 2009 **4693**
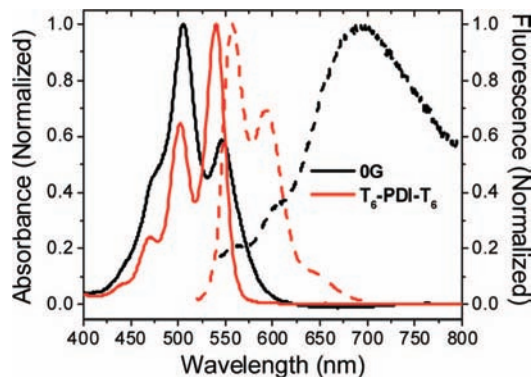
Figure 2. Normalized ground-state absorption (solid line) and emission (dashed) spectra of 1.0 μM **0G** and **T_6-PDI-T_6** in 10 mM sodium phosphate buffer and 100 mM NaCl (pH 7.4).

PDI$_2$-A: R = n-C$_8$H$_{17}$

PDI$_2$-B: R = CH(C$_{11}$H$_{23}$)$_2$

Figure 3. Structures of covalent, cofacial PDI dimers.

in 20 mM Tris buffer, 2 mM EDTA, 100 mM NaCl, pH 7.2, and 20% glycerol was loaded into quartz tubes (3.8 mm o.d., 2.4 mm i.d.) and subjected to several freeze–pump–thaw degassing cycles on a vacuum line (10^{-4} Torr). The tubes were then sealed with a hydrogen torch. TREPR measurements using continuous wave (CW) microwaves and direct detection were made using a Bruker Elexsys E580 X-Band EPR spectrometer outfitted with a variable Q dielectric resonator (ER-4118X-MD5-W1). The temperature was controlled by an Oxford Instruments CF935 continuous flow cryostat using liquid N$_2$. Samples were photoexcited at 532 nm (2.5 mJ/pulse, 7 ns, 10 Hz) using the frequency doubled output from a Nd:YAG laser (QuantaRay DCR-2). The polarization of the laser was set to 54.7° relative to the direction of the static magnetic field to avoid magneto-photoselection effects on the spectra. Following photoexcitation, kinetic traces of transient magnetization were accumulated under CW microwave irradiation (typically 6–20 mW). The field modulation was disabled to achieve a time response of $Q/\pi\nu \approx 30$ ns, where Q is the quality factor of the resonator and ν is the resonant frequency, while microwave signals in emission (e) and/or enhanced absorption (a) were detected in both the real and the imaginary channels (quadrature detection). Sweeping the magnetic field gave 2D spectra versus both time and magnetic field. For each kinetic trace, the signal acquired prior to the laser pulse was subtracted from the data. Kinetic traces recorded at magnetic field values off-resonance were considered background signals, whose average was subtracted from all kinetic traces. The spectra were subsequently phased into a Lorentzian part and a dispersive part, and the former, also known as the imaginary magnetic susceptibility χ'', is presented. BDPA (α,γ-bisdiphenylene-β-phenylallyl) dissolved in a polystyrene film and mounted into 0.8-mm-o.d. thin-walled quartz tubes was used as an internal standard for phase alignment of the EPR spectra. Simulation of the powder-pattern spectra of the spin-polarized RP signals[29] and the triplet states[30,31] resulting from charge recombination was performed using a home-written MATLAB program[32] following published procedures.

Results and Discussion

Steady-State Spectroscopy and Hairpin Dimer Structure. The visible absorption spectra of reference conjugate **T_6-PDI-T_6** and hairpin dimer **0G** are compared in Figure 2. The absorption spectrum of **T_6-PDI-T_6** displays a vibronic absorbance band ratio of $A^{0-0}/A^{0-1} = 1.5$, which is characteristic of the PDI monomer, and thus, this conjugate most likely adopts a random coil structure. In contrast, **0G** has $A^{0-0}/A^{0-1} = 0.67$, slightly red-shifted band maxima, and pronounced tailing of the
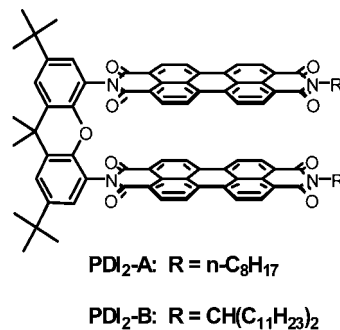
A^{0-0} band to longer wavelengths. The spectra of the other **nG** conjugates are similar to that of **0G** (Figure S1 in Supporting Information), and are consistent with dimerization of the **nG** hairpins by self-association of the PDI hairpin linkers. The association of the two PDI molecules is greatly assisted in the aqueous medium by their large hydrophobic surfaces.

A recent study of covalent, cofacial PDI dimers and trimers,[33] including **PDI$_2$-A** and **PDI$_2$-B** (Figure 3), has shown that their ground-state absorption spectra are very similar to those observed here for **nG**, and can be explained using the zero order molecular exciton model taking into account the effects of vibronic coupling.[34–41] In these dimers and trimers, the transition moments of the lowest energy electronic transitions of each PDI (polarized along the PDI N–N axis) are aligned approximately parallel to one another by covalent attachment to a xanthene spacer. In addition, previous circular dichroism studies and associated molecular dynamics simulations of PDI-linked DNA hairpins closely related to **nG** show that two hairpins dimerize by association of their PDI linkers and adopt a face-to-face geometry in which the long axes of the PDI molecules are approximately aligned with $\theta = \pm20°$.[24] On the basis of these results, the absorption spectra of PDI within **nG** strongly suggest that these hairpins also dimerize into a similar conformation.

The two closely associated PDI molecules within the **nG** dimers have significant exciton coupling. The energy of the lowest excited singlet state of the PDI monomer in **T_6-PDI-T_6** as determined from the energy average of the 0–0 bands of its absorption and emission spectra (Figure 2) is 2.26 eV. The absorption spectrum of the **0G** hairpin dimer shows that its exciton splitting ($2V$) is approximately 0.38 eV, so that the electronic absorption of the strongly disallowed lower exciton state of **0G** (and the other **nG** dimers) should occur at about 2.07 eV. Assuming that the Stokes shift following excitation is comparable to that of the PDI monomer, the energy of the lower exciton state of the **nG** dimers (^{1*}PDI$_2$) is estimated to be about 2.0 eV. The energies of the excimer-like states of **nG** (^{1*X}PDI$_2$) are even lower, since the emission maxima are all about 695 nm or 1.79 eV (see below). The approximate energy levels for the PDI monomer and dimer excited states are summarized in Figure 4.

The melting temperatures of the **nG** hairpins were determined from thermal dissociation profiles for either the 260 nm nucleobase absorption or the A^{0-0}/A^{0-1} band intensity ratio (Table S2 in Supporting Information). These measurements report on the unstacking of the hairpin base pairs and dissociation of the PDI dimers, respectively. Interestingly, these measurements show that both dissociative processes occur at the same values of $T_m = 65 \pm 2$ °C for the **nG** hairpins, where $n = 0–5$.

The fluorescence emission spectrum of **T_6-PDI-T_6** (Figure 2) is the mirror image of its absorption and fluorescence
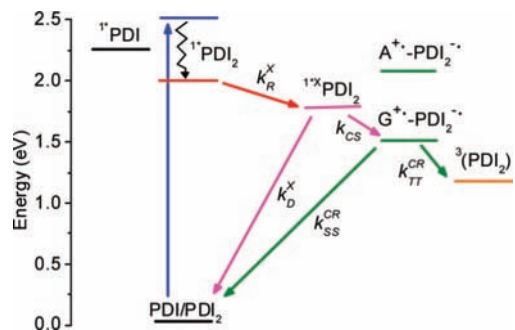
Figure 4. Energy levels for excited and charge transfer states of **nG** dimers.

excitation spectra, and is characteristic of PDI monomer fluorescence.[33] The fluorescence quantum yield of **T₆-PDI-T₆** ($\Phi_F = 0.15$) is somewhat reduced from the near unity quantum yield of monomeric PDI in organic solvents but is typical of PDI attached to single-stranded DNA having only pyrimidine nucleobases.[20] In contrast, the fluorescence spectrum of the **0G** hairpin dimer (Figure 2) is dominated by a broad band at 695 nm, which is similar to that observed for dimers **PDI₂-A** and **PDI₂-B** and is assigned to $^{1*X}PDI_2$.[33] The weak vibronic bands at 560 and 600 nm are attributed to a small amount of monomer hairpin (ca. 5%) present in equilibrium with the hairpin dimer under the conditions of these measurements. Similar weak emission spectra are observed for all the **nG** hairpin dimers (Figure S2 and Table S2 in Supporting Information). The fluorescence quantum yields and lifetimes of **0G**, **4G**, and **8G** ($\Phi_F = 0.003$ and $\tau_F = 1.2$ ns) are lower than those of monomeric PDI ($\Phi_F = 0.98$ and $\tau_F = 4.5$ ns[33]). Comparing our data for **PDI₂-A** and **PDI₂-B** with that for the **nG** hairpin dimers, both the fluorescence quantum yields and lifetimes of $^{1*X}PDI_2$ are

very sensitive to the PDI dimer geometry. For example, the *n*-octyl group in **PDI₂-A** is sterically less demanding than the branched 12-tricosanyl group in **PDI₂-B**, thus allowing geometric relaxation following photoexcitation to result in a closer approach of the two PDI molecules in **PDI₂-A**. This closer association results in a more highly red-shifted absorption maximum, lower fluorescence quantum yield, and shorter fluorescence lifetime for **PDI₂-A** relative to **PDI₂-B**. In a similar manner, the absence of covalent bonding between in the **nG** hairpin dimers allows them to relax into energy minimized geometries in which the two PDI molecules in $^{1*X}PDI_2$ are tightly associated, leading to low fluorescence quantum yields and short lifetimes.

Excited-State Spectroscopy. The transient absorption spectra of the hairpin dimers **0G**, **1G**, **2G**, and **4G** at several delay times following excitation with 505 nm, 130 fs laser pulses are shown in Figure 5. Transient spectra for the other **nG** hairpins are provided in Figure S3 in Supporting Information. In all cases, two transient spectral features are formed during the laser pulse, a negative band with minima near 505 and 546 nm resulting from ground-state depletion and an absorption feature at 570−800 nm.[42,43] The transient spectra between 440 and 800 nm and 0−6 ns were subjected to singular value decomposition and global fitting using a sum of exponentials to obtain the principal kinetic components and their associated spectra (insets, Figure 5 and Figure S3 in Supporting Information).[28] For each hairpin, with the exception of **1G**, the initial broad 570−800 nm absorption narrows rapidly ($\tau_1 = 10$−28 ps) into a band having a distinct maximum near 650 nm. This rapid narrowing is consistent with the spectra associated with τ_1 (insets, Figure 5 and Figure S3 in Supporting Information) in which the minima near 650 nm indicate that this band rises with τ_1, while the positive ΔA bands on either side of 650 nm decay with τ_1. The
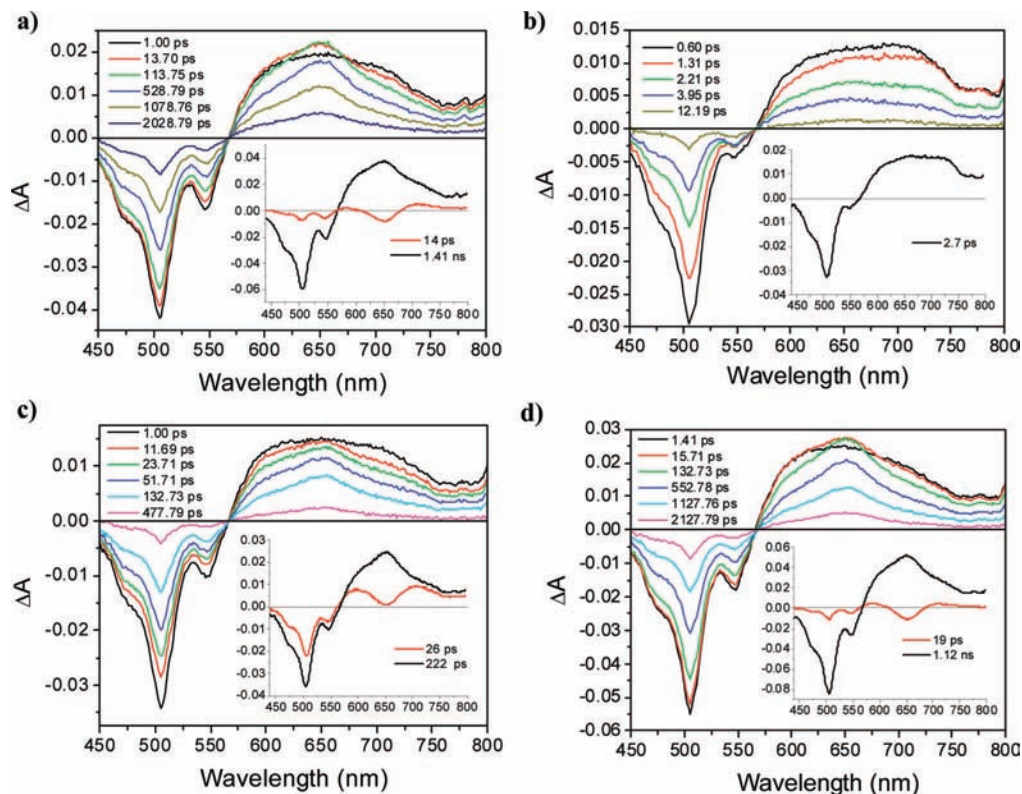
Figure 5. Transient absorption spectra of (a) **0G**, (b) **1G**, (c) **2G**, and (d) **4G**. Samples in buffer solution (10 mM phosphate buffer, 100 mM NaCl, pH 7.4) following excitation with 505 nm, 130 fs laser pulses. Insets: spectra associated with the kinetic components obtained by global analysis.

Charge Transport through DNA

J. Phys. Chem. A, Vol. 113, No. 16, 2009 **4695**

TABLE 1: Global Fits to Transient Absorption Kinetics for PDI-DNA Conjugates

conjugate	τ_1 (ps)[a]	τ_2 (ns)[b]
0G	14 ± 1	1.41 ± 0.23
1G	2.7 ± 0.3[b]	
2G	26 ± 1	0.22 ± 0.02
3G	19 ± 1	1.53 ± 0.03
4G	19 ± 1	1.12 ± 0.02
5G	10 ± 1	1.28 ± 0.02
8G	28 ± 1	1.39 ± 0.02
T_6-PDI-T_6	258 ± 26[b]	1.37 ± 0.06

[a] Rise at 650 nm and decay at 700 nm unless otherwise noted.
[b] Decay component at all wavelengths.

650 nm band then decays to $\Delta A = 0$ with $\tau_2 = 0.22-1.4$ ns with no significant band shape changes. The spectra associated with τ_2 (insets, Figure 5 and Figure S3 in Supporting Information) are all very similar with the negative bands rising (recovering) with τ_2 and the positive bands decaying with τ_2. For **1G**, the initial broad band decays rapidly ($\tau_1 = 2.7$ ps) before significant band shape changes occur. The time constants τ_1 and τ_2 for hairpins **nG** are summarized in Table 1. The transient decays appear to be largely complete on the 6 ns time scale of our measurements. Attempts to detect longer-lived transients from **0G**, **4G**, and **8G** using a nanosecond pulsed laser apparatus with an instrument response time of ca. 7 ns were unsuccessful.[20] The transient spectra for **T_6-PDI-T_6** are provided in Figure S3 in Supporting Information. In addition to the negative band with minima near 505 and 546 nm resulting ground-state depletion, **T_6-PDI-T_6** has an absorption maximum at 710, which is assigned to monomeric ^{1*}PDI.[33,44]

With the exception of **1G**, the time-dependent spectral narrowing of the 570−800 nm absorption bands of **nG** is similar to that observed for **PDI$_2$-A** and **PDI$_2$-B** in organic solvents. Photoexcitation of **PDI$_2$-A** and **PDI$_2$-B** as well as the **nG** dimers into their upper exciton states results in rapid nonradiative decay to ^{1*}PDI$_2$ in times faster than our 180 fs IRF. The ^{1*}PDI$_2$ states then undergo a geometry change to produce the relaxed ^{1*X}PDI$_2$ states. The transient absorption spectra of **PDI$_2$-A** narrow rapidly ($\tau = 1.2$ ps), while those of **PDI$_2$-B** narrow significantly more slowly ($\tau = 69$ ps). In the latter case, we concluded that the bulky 12-tricosanyl groups slow the motions necessary for the two PDI molecules within **PDI$_2$-B** to achieve the optimal relaxed geometry to stabilize ^{1*X}PDI$_2$. The time scale of the narrowing for the **nG** hairpin dimers is similar to that for **PDI$_2$B** even though there are no nonbonded interactions between the two hairpins. The time scale of the observed spectral narrowing is sufficiently slow that it does not result from vibrational cooling,

although a small contribution to the overall narrowing cannot be ruled out for times <15 ps. Engel and co-workers[41] have recently proposed that an excited, unconstrained PDI dimer can undergo a torsional angle change from ~30° in ^{1*}PDI$_2$ to ~0° in ^{1*X}PDI$_2$. A reduction in the torsional angle θ between the two PDI molecules within the **nG** hairpin dimers from ~20° to ~0° as ^{1*}PDI$_2 \rightarrow {}^{1*X}$PDI$_2$ requires a substantial change in solvent reorganization, which would account for the relatively slow spectral narrowing of their transient absorption spectra.[45]

Charge Transfer. The PDI chromophore is a strong photochemical oxidant and has been widely employed in studies of photoinduced electron transfer.[27,42,46−56] From our previously reported work on PDI monomers serving as base-pair surrogates within DNA duplex structures,[20] it is clear that monomeric ^{1*}PDI is fully capable of injecting holes into A-tracts as well as oxidizing G. The lower excited-state energies of ^{1*}PDI$_2$ and ^{1*X}PDI$_2$ in the **nG** hairpin dimers (Figure 4) have important consequences for possible charge transfer mechanisms within **nG**. The free energies of charge separation, ΔG_{CS}, and charge recombination, ΔG_{CR}, within **nG** were estimated using Weller's expression[57] based on the Born dielectric continuum model of the solvent to determine the energy of formation of an ion pair, ΔG_{IP}, in a solvent of arbitrary polarity

$$\Delta G_{IP} = E_{OX} - E_{RED} - \frac{e^2}{r_{DA}\varepsilon_S} + e^2\left(\frac{1}{2r_1} + \frac{1}{2r_2}\right)\left(\frac{1}{\varepsilon_S} - \frac{1}{\varepsilon_{SP}}\right) \quad (1)$$

$$\Delta G_{CS} = \Delta G_{IP} - E_S \quad (2)$$

$$\Delta G_{CR} = -\Delta G_{IP} \quad (3)$$

where E_{OX} is the nucleobase oxidation potential (1.24 V for G, 1.69 V for A, and ca. 1.9 V for T or C vs SCE in acetonitrile)[58] and E_{RED} is the reduction potential of PDI$_2$ (-0.58 V vs SCE in CH$_2$Cl$_2$ as determined from the corresponding covalent, cofacial dimer[59]) measured in a solvent having dielectric constant ε_{SP} (in this case $\varepsilon_{SP} = 38$ and 9 for CH$_3$CN and CH$_2$Cl$_2$, respectively), e is the charge of the electron, r_1 and r_2 are the effective ionic radii of the radical ions, r_{DA} is the donor−acceptor distance, ε_S is the static dielectric constant of the solvent in which the spectroscopy is performed, and E_S is the energy of the relevant photoexcited singlet state of PDI$_2$. Assuming a moderately
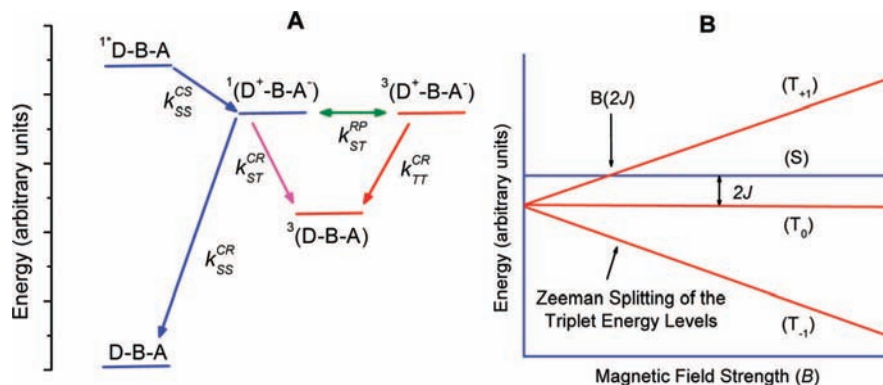
Figure 6. (A) Electron transfer and intersystem crossing pathways in a donor−bridge−acceptor (D−B−A) system. (B) Radical ion pair energy levels as a function of magnetic field for $2J > 0$, $D = 0$.

polar environment for the interior of DNA ($\varepsilon_S \sim 10$),[60,61] oxidation of nucleobase donors adjacent to $^{1*}PDI_2$ or $^{1*X}PDI_2$, where $r_{DA} \cong 3.5$ Å and the effective ionic radii r_1 and r_2 are both $r_{DA}/2$, should be exergonic for G, and endergonic for A, T, and C (Figure 4). Thus, the inability of $^{1*}PDI_2$ and $^{1*X}PDI_2$ to oxidize nucleobases other than G should result in the dominance of superexchange-mediated charge transfer in the **nG** hairpin dimers, so that the charge transfer efficiency should decrease strongly with G-PDI$_2$ distance.

Once the initial spectral narrowing of the 570−800 nm band has occurred, indicating that $^{1*X}PDI_2$ has formed, all of the **nG** hairpin dimers except **1G** have similar transient absorption spectra. Moreover, with the exception of **1G** and **2G**, they also have similar decay time constants ($\tau_2 = 1.12-1.41$ ns). Since electron transfer from A, C, and T nucleobases to $^{1*X}PDI_2$ is precluded for energetic reasons, the nearly constant decay time constants of this state, when G is far from $^{1*X}PDI_2$ (or absent in the case of **0G**), strongly suggest that these time constants are the intrinsic decay times of $^{1*X}PDI_2$. On the other hand, for **1G**, electron transfer from the adjacent G to $^{1*}PDI_2$ is faster than the transition from $^{1*}PDI_2$ to $^{1*X}PDI_2$. However, the transient absorption spectrum of **1G** (Figure 5b) does not have a distinct absorption near 725 nm, which is diagnostic for PDI$^{-\bullet}$.[62] The failure to observe a change in the transient absorption spectrum upon electron transfer from G to $^{1*}PDI_2$ is indicative of inverted kinetics, in which charge recombination occurs with a rate constant comparable to or faster than charge separation. We have previously observed inverted kinetics for charge separation and charge recombination in perylenediamide-linked hairpins having guanine or dezaguanine as hole acceptors.[63] Similar behavior is observed for **2G**, except that in this case electron transfer from G to $^{1*}PDI_2$ is slower than the transition from $^{1*}PDI_2$ to $^{1*X}PDI_2$ (220 ps vs 26 ps). Once again, inverted kinetics prevail, as indicated by the invariance of the spectrum of $^{1*X}PDI_2$ during its decay. Electron transfer from G to $^{1*X}PDI_2$ competes poorly with the intrinsic decay of $^{1*X}PDI_2$ in **3G**, **4G**, **5G**, and **8G** as a result of the steep exponential distance dependence of superexchange-mediated electron transfer. Nevertheless, as we will discuss below, low yields of RPs can be detected by TREPR even for **4G** by taking advantage of their strong spin polarization.

Radical Pair TREPR Spectra. TREPR measurements were used to determine whether photoexcitation of the **nG** hairpin dimers results in the formation of RPs. If charge separation within a donor−bridge−acceptor (D−B−A) system initially forms a singlet RP, $^1(D^{+\bullet}-B-A^{-\bullet})$, it may undergo RP-ISC[64,65] to produce the triplet RP, $^3(D^{+\bullet}-B-A^{-\bullet})$ (Figure 6A). TREPR measurements were carried out in a 350 mT magnetic field, so that the triplet sublevels of $^3(D^{+\bullet}-B-A^{-\bullet})$ undergo Zeeman splitting (Figure 6B) and are best described by the T_{+1}, T_0, and T_{-1} eigenstates that are quantized along the applied magnetic field.[23,66−68] RP-ISC depends on both the spin−spin exchange interaction, $2J$, and the dipolar interaction, D, between the two radicals that comprise the RP. When the spin−spin interactions $2J$ and D are small, generally for distances >~10−15 Å, the RP-ISC mechanism results in formation of a spin-correlated radical pair (SCRP).[64,65,69,70] Under these conditions, the S and T_0 spin states of the RP are close in energy and mix, while the T_{+1} and T_{-1} states are energetically far removed from T_0 and do not mix with S.[23,66−68]

Neglecting hyperfine interactions, the SCRP spectrum consists of two antiphase doublets, centered at the *g*-factor of the individual radicals of the pair. The splitting of each doublet is

determined by $2J$ and D. Resolved hyperfine interactions lead to further splitting of the doublet for each radical. The experimentally observed SCRP spectrum is a superposition of the four line spectra for all possible orientations of the RP, with respect to the external magnetic field, B_0. The positions (ω_{ij}) of the four EPR transitions for the SCRP are[64,65,69,70]

$$\omega_{12} = \omega_0 - \Omega - J + D_{zz} \tag{4}$$

$$\omega_{34} = \omega_0 - \Omega + J - D_{zz}$$

$$\omega_{13} = \omega_0 + \Omega - J + D_{zz}$$

$$\omega_{24} = \omega_0 + \Omega + J - D_{zz}$$

where ω_0 is the center of the spectrum and

$$\Omega^2 = (J + D_{zz}/2)^2 + Q^2 \tag{5}$$

and

$$D_{zz} = D[3\cos^2(\xi) - 1] \tag{6}$$

where ξ is the angle between the dipolar axis of the radical pair and the direction of the magnetic field B_0. The mixing term Q between singlet and triplet states is

$$Q = \frac{1}{2}(g_1 - g_2)\beta B_0/\hbar + \frac{1}{2}(\sum a_{1i}m_{1i} - \sum a_{2j}m_{2j}) \tag{7}$$

where g_1 and g_2 are the g factors of radicals 1 and 2, a_{1i} and a_{2j} are the hyperfine coupling constants of radicals 1 and 2 having m_{1i} and m_{2j} nuclei. The intensities of the transitions are

$$-I_{12} = -I_{13} = I_{24} = I_{34} = Q^2/(4\Omega^2) \tag{8}$$

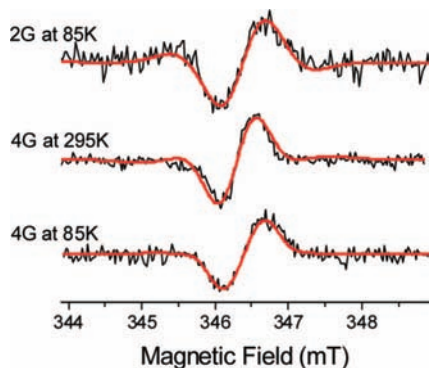The electron spin polarization (ESP) pattern of the EPR signal is determined by the sign rule

$$\Gamma = \mu \, \text{sign}[J - D(3\cos^2(\xi) - 1)] = \begin{cases} (-) \text{ gives } e/a \\ (+) \text{ gives } a/e \end{cases} \tag{9}$$

where μ is -1 or $+1$ for singlet or triplet excited states precursor, respectively, and a is enhanced absorption and e is emission, respectively.

The magnitude of J depends exponentially on the distance r between the two radicals and is assumed to be isotropic, while that of D depends on $1/r^3$ and is anisotropic. For large molecules in solution, such as the hairpins studied here, and for molecules in the solid state, D is not rotationally averaged to zero. D is usually approximated using the point dipole model[71]

$$D = -\frac{3\mu_0 g_e^2 \beta_e^2}{8\pi r^3} \tag{10}$$

where μ_0, g_e, and β_e are the vacuum permeability, electronic g-factor, and Bohr magneton, respectively. In units of mT and Å, $D = -2785$ mT·Å/r^3. The two RP states that result from

Charge Transport through DNA

J. Phys. Chem. A, Vol. 113, No. 16, 2009 **4697**

Figure 7. TREPR spectra of **2G** and **4G** 85 K and at 295K (for **4G**) at 100 ns following a 532 nm, 2.5 mJ laser pulse. The smooth curves superimposed on the experimental spectra are computer simulations of the radical pair spectra with the parameters given in Table 2.

TABLE 2: RP Simulation Parameters for 2G and 4G at 100 ns after the Laser Pulse

conjugate	T (K)	$2J$ (mT)	D (mT)	r (Å)	k_{SS}^{CR} (10^6 s^{-1})	k_{TT}^{CR} (10^6 s^{-1})
2G	85	0.02 ± 0.01	-6.6 ± 0.1	7.5 ± 0.1	6 ± 1	12 ± 1
4G	295	0.06 ± 0.01	-1.2 ± 0.1	13.2 ± 0.1	5 ± 1	18 ± 1
4G	85	0.06 ± 0.01	-1.0 ± 0.1	14.1 ± 0.1	5 ± 1	14 ± 1

S-T_0 mixing are preferentially populated due to the initial population of S, so that the four $\Delta m = \pm 1$ EPR transitions that occur between these two mixed states and T_{+1} and T_{-1} display an intensity pattern characteristic of the strong spin polarization.[64,65]

Following photoexcitation with a 532 nm, 7 ns laser pulse, spin-polarized RP signals are observed for **2G** at 85 K and **4G** at 85 and 295 K (Figure 7). No RP spectrum was observed for **2G** at 295 K, probably because charge recombination back to singlet ground state is very fast. Since the rates of charge separation and recombination frequently slow considerably upon freezing the solvent to its glassy state,[72] the appearance of a signal for **2G** at 85 K is also reasonable. In addition, no RP spectrum was observed for **0G** and **8G** under any conditions. This is consistent with the inability of ^{1*X}PDI$_2$ to oxidize A, C, and T in all **nG** hairpin dimers, as well as the long distance between G and PDI$_2$ in **8G**. Since the g factors of both radicals are similar, significant overlap of the two antiphase doublets results in one dominant doublet having an e/a spin polarization pattern. The spectra were simulated using the SCRP model of Till and Hore[29] and the hyperfine coupling constants measured for G$^{+\bullet}$[73] and PDI$^{-\bullet}$.[74] The model accounts for the spin selective decay rates of the singlet and triplet RPs, k_{SS}^{CR} and k_{TT}^{CR}, respectively (Figure 6A).[29] The fits to the data are given in Figure 7, while the fitting parameters are summarized in Table 2. Since charge separation in dimer hairpins **2G** and **4G** proceeds from ^{1*X}PDI$_2$ and the resultant RP spectra exhibit an (e, a) spin polarization pattern, eq 9 restricts the signs and magnitudes that 2J and D can adopt. Given that D is negative (eq 10), if 2J > 0, eq 9 predicts an (e, a) pattern for all values of 2J and D, while if 2J < 0, eq 9 predicts an (e, a) pattern only when $|D|$ > $|2J|$.[64,65]

The G$^{+\bullet}$−PDI$_2^{-\bullet}$ distances for **2G** and **4G** at 85 K obtained using D from the simulations and eq 10 are 7.5 and 14.1 Å, respectively (Table 2). These values are in reasonable agreement with the average spacing of 3.5 Å between the π-stacked base pairs. The slightly decreased distance for **4G** at 295 K may indicate increased hairpin flexibility in solution that allows conformational relaxation of G$^{+\bullet}$−PDI$_2^{-\bullet}$.

The value of 2J depends exponentially on the distance between the two radical ions, so that 2J is small when the distance r is large, and can be described by[75]

$$2J = 2J_0 e^{-\alpha(r-r_0)} \tag{11}$$

where 2J_0 is the spin−spin exchange interaction at van der Waals contact, α is a constant, and r_0 is the van der Waals contact distance of about 3.5 Å. The spin−spin exchange interaction 2J is directly proportional to the electronic coupling matrix element V^2 for the charge recombination reaction.[76−78] In turn, electron transfer theory shows that the rate constant k^{CR} for charge recombination is also directly proportional to V^2,[79,80] so that k^{CR} is directly proportional to 2J. The values of 2J for **2G** and **4G** (Table 2) are very small and imply that the noncovalent electronic interaction of G$^{+\bullet}$ and PDI$_2^{-\bullet}$ through the intervening A-T π-stacked base pairs is weak, which is consistent with the relatively slow charge recombination observed here for G$^{+\bullet}$-PDI$_2^{-\bullet}$ and with our earlier results on electron transfer in DNA hairpins using PDI base-pair surrogates.[20] Even though G$^{+\bullet}$ and PDI$_2^{-\bullet}$ are much closer in **2G** than in **4G**, 2J for **2G** is smaller than that of **4G** at 85 K. This apparent deviation from the behavior predicted by eq 11 most likely derives from differing values of 2J_0 for each molecule resulting from differences in electronic interactions between the intervening π-stacked nucleobases due to the helical pitch of the DNA duplex. The value of 2J for **4G** does not show a temperature dependence within experimental uncertainty, which implies that only small conformational changes occur with temperature, and is consistent with the small changes observed for D as well. In addition, the lack of temperature dependence of both k_{SS}^{CR} and k_{TT}^{CR} suggests that $\Delta G_{CR} \cong \lambda$ for both processes, where λ is the total reorganization energy for the charge recombination.[79]

TREPR Spectra of Triplet States Resulting from Charge Recombination. The non-Boltzmann spin distribution within the SCRP is transferred to the neutral triplet state ^{3*}(D−B−A) that results from radical ion pair recombination within ^{3}(D$^{+\bullet}$−B−A$^{-\bullet}$) as shown in Figure 6A.[21,81] The main features of the EPR spectrum of ^{3*}(D−B−A) are determined mainly by the Zeeman interaction and the zero field splitting (ZFS), which arises as a result of the dipole−dipole interaction between the two unpaired electrons in the triplet state. The nuclear hyperfine couplings within the triplet state are rarely, if ever, seen in randomly oriented triplets in an external magnetic field because of the large anisotropy. The total spin Hamiltonian describing the Zeeman and the ZFS interactions is

$$H_T = \beta_e B_0 \cdot \mathbf{g} \cdot \mathbf{S} + \mathbf{S} \cdot \mathbf{D} \cdot \mathbf{S} \tag{12}$$

where β_e is the Bohr magneton, B_0 is the applied magnetic field, **g** is the electronic g-tensor, **S** is the spin operator, and **D** is the ZFS tensor. When **D** is traceless, the ZFS term can be expressed, with just two parameters as

$$\mathbf{S} \cdot \mathbf{D} \cdot \mathbf{S} = D\left(S_z^2 - \frac{1}{3}S^2\right) + E(S_x^2 - S_y^2) \tag{13}$$

where D is

$$D = D_{ZZ} - \frac{1}{2}(D_{xx} - D_{yy}) \tag{14}$$

and E is

$$E = \frac{1}{2}(D_{xx} - D_{yy}) \qquad (15)$$

where E is the rhombic term that is present, when the symmetry is lower than axial. The effect of the ZFS term is to lift the degeneracy of the triplet manifold in the absence of an external magnetic field as a function of the symmetry of the molecule.

The triplet line shape for randomly oriented systems has been described earlier.[30,31,82] When the applied magnetic field is along one of the principal axes of the triplet state, one triplet sublevel remains stationary with respect to the field strength. The energies of the two other sublevels diverge in opposite directions as the magnetic field increases (Figure 6B). In the high magnetic field limit, the electron spins are quantized along the axis of the applied field into T_+, T_0, and T_- states (corresponding to the $+1$, 0, and -1 projections of S along B, respectively).

The anisotropy of the ZFS, in general, leads to six observable lines or turning points around the $g = 2$ region, Z_2, X_1, Y_1, Y_2, X_2, and Z_1 going from low field to high field. Assuming that $D > 0$, which is the usual assumption for flat planar aromatics, the $|0\rangle \leftrightarrow |+1\rangle$ transition has components at a field position displaced from the field position of the free electron ($h\nu/g_e\beta_e$) by $-D$, $+(D - 3E)/2$ and $+(D + 3E)/2$. Likewise, the $|0\rangle \leftrightarrow |-1\rangle$ transition has lines at field positions displaced from g by $+D$, $-(D - 3E)/2$ and $-(D + 3E)/2$, respectively. Thus, the ZFS parameters can be extracted from the resulting powder spectrum, and are $\Delta H_z = 2|D|$, $\Delta H_x = |D| + 3|E|$ and $\Delta H_y = |D| - 3|E|$, where ΔH_i ($i = x, y, z$) are the field differences of the pairs of transitions.

TREPR spectra of **0G**, **2G**, **4G**, and **8G** were measured at 85 K and at 25 K (data not shown), and the spectra show the same features for both temperatures at 500 ns following a 532 nm, 7 ns laser pulse (Figure 8). All spectra feature a broad triplet signal with a width of ~92 mT, having an electron spin polarization (ESP) pattern of (e, e, e, a, a, a) and a narrow RP spectrum at $g \sim 2$ for **2G** and **4G**, which was discussed previously. The triplet lineshapes were simulated using a linear combination of RP-ISC and spin−orbit-induced intersystem crossing (SO-ISC) mechanisms. The simulations indicate that SO-ISC is the main source of ^{3*}PDI and there is no contribution from RP-ISC for **0G** and **8G**. In contrast, the triplet spectra of **2G** and **4G** have a small contribution from RP-ISC with **4G** having the higher percentage contribution. The relative population rates for SO-ISC favor the T_x sublevel over T_y or T_z. The results of the fitting parameters are summarized in Table 3.

The fluorescence quantum yield of monomeric PDI is approximately unity,[46] so that the yield of ^{3*}PDI produced directly from ^{1*}PDI is insignificant. Following photoexcitation, no triplet EPR spectra are observed for monomeric PDI at the same concentration as the **nG** hairpin dimers. In the absence of electron transfer, photoexcitation of **0G** and **8G** produce reasonably intense triplet EPR signals. The observed magnitudes of D and E are very similar to those of monomeric ^{3*}PDI generated previously by high yield RP-ISC in donor−acceptor compounds,[23] while the observed (e, e, e, a, a, a) ESP pattern is strictly due to a SO-ISC process. Recently, Veldman et al.[59] reported enhanced intersystem crossing yields of ^{3*}PDI within compounds related to **PDI$_2$-A** and **PDI$_2$-B**. They proposed that a significant charge transfer interaction in ^{1*}PDI$_2$ leads to enhanced SO-ISC producing 20−80% triplet yields depending on solvent. The relatively small contribution of the RP-ISC mechanism to the triplet signal for **2G** and **4G** can be explained by the low quantum yield of RP formation for **nG**, when $n > 1$, combined with structurally related variations in $2J$ and D, which
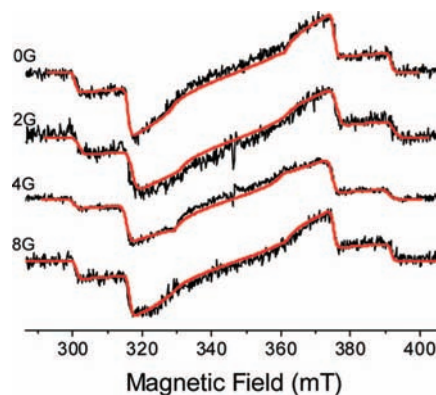
Figure 8. Triplet TREPR spectra of the DNA hairpins recorded at 85 K and 500 ns following a 7 ns, 532 nm laser pulse. The smooth curves superimposed on the experimental spectra are computer simulations of the triplet spectra with the parameters given in Table 3.

TABLE 3: Zero Field Splitting Parameters and Relative Population Rates As Obtained from Simulations of Triplet State

hairpin	D (mT)	E (mT)	A_x	A_y	A_z	SO-ISC (%)	RP-ISC (%)
0G	45.56	−4.63	0.803	0.489	0.249	100	0
2G	45.34	−4.58	0.794	0.510	0.218	95	5
4G	45.41	−4.65	0.799	0.496	0.240	79	21
8G	45.70	−4.58	0.819	0.496	0.222	100	0

modulate the spin-polarization of $G^{+\bullet}$-$PDI_2^{-\bullet}$. Low quantum yields of $G^{+\bullet}$−$PDI_2^{-\bullet}$ formation are strongly implied by the inability to observe any significant decrease in the lifetime of ^{1*X}PDI$_2$ for **3G-8G** and by the apparent inverted kinetics for both **1G** and **2G**. As mentioned above, low yields of RPs can be observed, provided that they exhibit strongly spin-polarized EPR spectra, as is clearly the case for both **2G** and **4G**.

The RP-ISC contribution to the ^{3*}PDI EPR spectra for **2G** and **4G** was simulated with an overall (a, e, e, a, a, e) ESP phase pattern, which is diagnostic of spin-selective charge recombination of a SCRP.[21] Interestingly, the ^{3*}PDI EPR spectrum of **4G** has a larger contribution from RP-ISC than does **2G**, even though the longer G-PDI distance in **4G** should lead to a much lower quantum yield of RP formation. It is important to recognize that ^{3*}PDI acquires spin polarization by both the SO-ISC and RP-ISC mechanisms and that the relative non-Boltzmann populations of the spin states responsible for the polarization do not generally reflect the overall quantum yield of RP formation. The data in Table 2 indicate that the spin-selective charge recombination rates of the RPs produced by RP-ISC in **2G** and **4G** at 85 K are essentially the same. This is most likely a consequence of the modulation of the electronic coupling matrix element by changes in π-stacking of the intervening bases due to the helical nature of the DNA duplex. If the A-T base pairs between G and PDI were all parallel and π-stacked, the predicted charge recombination rate of **4G** should be slower than that of **2G**. Equations 5 and 8 show that the EPR transition intensities for the spin-polarized RP states, which reflect the relative non-Boltzmann spin populations of these states, depend on J and D. As these quantities decrease, the transition intensities increase. The polarization of the S-T_0 mixed RP states is carried over directly to the T_0 sublevel of the ^{3*}PDI recombination triplet, which implies that for a given yield of RP, the spin-polarized ^{3*}PDI signal from **4G** should have a greater contribution from RP-ISC than **2G** provided that the exponential decrease in quantum

Charge Transport through DNA

J. Phys. Chem. A, Vol. 113, No. 16, 2009 **4699**

yield of RP with distance does not make the RP yield so small that the effects of spin polarization cannot compensate for it.

Conclusions

The optical absorption spectra of the **nG** hairpin dimers strongly suggest that the long (N−N) axes of their two π-stacked PDI molecules have torsional angles $\theta \simeq 20°$ in their ground states, similar to other structurally related PDI dimer hairpins. Photoexcitation of the **nG** hairpin dimers results in subpicosecond formation of $^{1*}PDI_2$ followed by structural relaxation of the PDI dimer to form the excimer-like state $^{1*X}PDI_2$ for which $\theta \simeq 0°$. Both of these states are lower in energy than $^{1*}PDI$, so that neither can oxidize A, C, and T. Electron transfer from G to $^{1*}PDI_2$ is faster than formation of $^{1*X}PDI_2$ only for **1G**. Electron transfer from G to $^{1*X}PDI_2$ for **2G-8G** occurs by the superexchange mechanism and thus becomes exponentially less efficient as the G-PDI$_2$ distance increases. Nevertheless, TREPR studies show that photoexcitation of **2G** and **4G** produce spin-correlated radical ion pairs having electron spin polarization patterns indicating that a low yield of charge separation proceeds by the reaction G-$^{1*X}PDI_2 \rightarrow {}^1(G^{+\bullet}\text{-}PDI_2{}^{-\bullet})$, which then undergoes RP-ISC to give $^3(G^{+\bullet}\text{-}PDI_2{}^{-\bullet})$. The strong spin-polarization of the RPs makes it possible to observe them, even when their concentration is low. When the **nG** hairpin dimers are excited at 85 K in a glassy buffer solution, an intense EPR spectrum due to $^{3*}PDI$ is observed. The triplet EPR spectrum results from two competing mechanisms. The dominant mechanism is enhanced SO-ISC, which occurs in all the hairpins examined. A minor contributor in **2G** and **4G** is $^{3*}PDI$ produced by charge recombination of RPs generated by the RP-ISC mechanism.

Supporting Information Available: Experimental details including DNA melting temperatures, fluorescence quantum yields, absorption and emission spectra, and transient absorption data. This material is available free of charge via the Internet at http://pubs.acs.org.

References and Notes

(1) Eley, D. D.; Spivey, D. I. T. *Trans. Faraday Soc.* **1962**, *58*, 411–415.

(2) Murphy, C. J.; Arkin, M. R.; Ghatlia, N. D.; Bossmann, S.; Turro, N. J.; Barton, J. K. *Proc. Natl. Acad. Sci. U.S.A.* **1994**, *91*, 5315–5319.

(3) Arkin, M. R.; Stemp, E. D. A.; Holmlin, R. E.; Barton, J. K.; Hormann, A.; Olson, E. J. C.; Barbara, P. F. *Science* **1996**, *273*, 475–480.

(4) Turro, N. J.; Barton, J. K. *J. Biol. Inorg. Chem.* **1998**, *3*, 201–209.

(5) Ly, D.; Sanii, L.; Schuster, G. B. *J. Am. Chem. Soc.* **1999**, *121*, 9400–9410.

(6) Nunez, M. E.; Hall, D. B.; Barton, J. K. *Chem. Biol.* **1999**, *6*, 85–97.

(7) Murphy, C. J.; Arkin, M. R.; Jenkins, Y.; Ghatlia, N. D.; Bossmann, S. H.; Turro, N. J.; Barton, J. K. *Science* **1993**, *262*, 1025–1029.

(8) Kelley, S. O.; Holmlin, R. E.; Stemp, E. D. A.; Barton, J. K. *J. Am. Chem. Soc.* **1997**, *119*, 9861–9870.

(9) Lewis, F. D.; Wu, T.; Zhang, Y.; Letsinger, R. L.; Greenfield, S. R.; Wasielewski, M. R. *Science* **1997**, *277*, 673–676.

(10) Meade, T. J.; Kayyem, J. F. *Angew. Chem., Int. Ed. Engl.* **1995**, *34*, 352–354.

(11) Lewis, F. D.; Zhu, H.; Daublain, P.; Cohen, B.; Wasielewski, M. R. *Angew. Chem., Int. Ed.* **2006**, *45*, 7982–7985.

(12) Lewis, F. D.; Wu, Y.; Zhang, L.; Zuo, X.; Hayes, R. T.; Wasielewski, M. R. *J. Am. Chem. Soc.* **2004**, *126*, 8206–8215.

(13) Takada, T.; Kawai, K.; Cai, X.; Sugimoto, A.; Fujitsuka, M.; Majima, T. *J. Am. Chem. Soc.* **2004**, *126*, 1125–1129.

(14) Kawai, K.; Takada, T.; Tojo, S.; Fujitsuka, M.; Majima, T. *J. Am. Chem. Soc.* **2003**, *125*, 6842–6843.

(15) Ottaviani, M. F.; Ghatlia, N. D.; Bossmann, S. H.; Barton, J. K.; Durr, H.; Turro, N. J. *J. Am. Chem. Soc.* **1992**, *114*, 8946–8952.

(16) Schiemann, O.; Turro, N. J.; Barton, J. K. *J. Phys. Chem. B* **2000**, *104*, 7214–7220.

(17) Yavin, E.; Boal, A. K.; Stemp, E. D. A.; Boon, E. M.; Livingston, A. L.; O'Shea, V. L.; David, S. S.; Barton, J. K *Proc. Natl. Acad. Sci. U.S.A.* **2005**, *102*, 3546–3551.

(18) Yavin, E.; Stemp, E. D. A.; O'Shea, V. L.; David, S. S.; Barton, J. K *Proc. Natl. Acad. Sci. U.S.A.* **2006**, *103*, 3610–3614.

(19) Nakajima, S.; Akiyama, K.; Kawai, K.; Takada, T.; Ikoma, T.; Majima, T.; Tero-Kubota, S. *ChemPhysChem* **2007**, *8*, 507–509.

(20) Zeidan, T. A.; Carmieli, R.; Kelley, R. F.; Wilson, T. M.; Lewis, F. D.; Wasielewski, M. R. *J. Am. Chem. Soc.* **2008**, *130*, 13945–13955.

(21) Levanon, H.; Norris, J. R. *Chem. Rev.* **1978**, *78*, 185–198.

(22) Shaakov, S.; Galili, T.; Stavitski, E.; Levanon, H.; Lukas, A.; Wasielewski, M. R. *J. Am. Chem. Soc.* **2003**, *125*, 6563–6572.

(23) Dance, Z. E. X.; Mi, Q. X.; McCamant, D. W.; Ahrens, M. J.; Ratner, M. A.; Wasielewski, M. R. *J. Phys. Chem. B* **2006**, *110*, 25163–25173.

(24) Zheng, Y.; Long, H.; Schatz, G. C.; Lewis, F. D. *Chem. Commun.* **2005**, 4795–4797.

(25) Letsinger, R. L.; Wu, T. F. *J. Am. Chem. Soc.* **1995**, *117*, 7323–7328.

(26) Rahe, N.; Rinn, C.; Carell, T. *Chem. Commun.* **2003**, 2120–2121.

(27) Rybtchinski, B.; Sinks, L. E.; Wasielewski, M. R. *J. Phys. Chem. A* **2004**, *108*, 7497–7505.

(28) *Surface Xplorer*; Ultrafast Systems LLC: Sarasota, FL.

(29) Till, U.; Hore, P. J. *Mol. Phys.* **1997**, *90*, 289–296.

(30) Kottis, P.; Lefebvre, R. *J. Chem. Phys.* **1963**, *39*, 393–403.

(31) Wasserman, E.; Snyder, L. C.; Yager, W. A. *J. Chem. Phys.* **1964**, *41*, 1763–1772.

(32) *MATLAB*; The MathWorks, Inc.: Natick, MA, 2006.

(33) Giaimo, J. M.; Lockard, J. V.; Sinks, L. E.; Scott, A. M.; Wilson, T. M.; Wasielewski, M. R. *J. Phys. Chem. A* **2008**, *112*, 2322–2330.

(34) Kasha, M.; Rawles, H. R.; El-Bayoumi, M. L. *Pure Appl. Chem.* **1965**, *11*, 371–392.

(35) Fulton, R. L.; Gouterman, M. *J. Chem. Phys.* **1964**, *41*, 2280–2286.

(36) Oddos-Marcel, L.; Madeore, F.; Bock, A.; Neher, D.; Ferencz, A.; Rengel, H.; Wegner, G.; Kryschi, C.; Trommsdorff, H. P. *J. Phys. Chem.* **1996**, *100*, 11850–11856.

(37) Myers-Kelley, A. *J. Chem. Phys.* **2003**, *119*, 3320–3331.

(38) Seibt, J.; Marquetand, P.; Engel, V.; Chen, Z.; Dehm, V.; Würthner, F. *Chem. Phys.* **2006**, *328*, 354–362.

(39) Seibt, J.; Dehm, V.; Würthner, F.; Engel, V *J. Chem. Phys.* **2007**, *126*, 164308/164301–164308/164306.

(40) Clark, A. E.; Qin, C.; Li, A. D. Q. *J. Am. Chem. Soc.* **2007**, *129*, 7586–7595.

(41) Fink, R. F.; Seibt, J.; Engel, V.; Renz, M.; Kaupp, M.; Lochbrunner, S.; Zhao, H.-M.; Pfister, J.; Würthner, F.; Engels, B. *J. Am. Chem. Soc.* **2008**, *130*, 12858–12859.

(42) van der Boom, T.; Hayes, R. T.; Zhao, Y. Y.; Bushard, P. J.; Weiss, E. A.; Wasielewski, M. R. *J. Am. Chem. Soc.* **2002**, *124*, 9582–9590.

(43) Rybtchinski, B.; Sinks, L. E.; Wasielewski, M. R. *J. Phys. Chem. A* **2004**, *108*, 7497–7505.

(44) Gosztola, D.; Niemczyk, M. P.; Svec, W. A.; Lukas, A. S.; Wasielewski, M. R. *J. Phys. Chem. A* **2000**, *104*, 6545–6551.

(45) Furse, K. E.; Corcelli, S. A. *J. Am. Chem. Soc.* **2008**, *130*, 13103–13109.

(46) Ford, W. E.; Kamat, P. V. *J. Phys. Chem.* **1987**, *91*, 6373–6380.

(47) Ford, W. E.; Hiratsuka, H.; Kamat, P. V. *J. Phys. Chem.* **1989**, *93*, 6692–6696.

(48) Würthner, F.; Thalacker, C.; Sautter, A. *Adv. Mater.* **1999**, *11*, 754–758.

(49) Langhals, H.; Saulich, S *Chem. Eur. J.* **2002**, *8*, 5630–5643.

(50) Schenning, A. P. H. J.; van Herrikhuyzen, J.; Jonkheijm, P.; Chen, Z.; Würthner, F.; Meijer, E. W. *J. Am. Chem. Soc.* **2002**, *124*, 10252–10253.

(51) Kirmaier, C.; Hindin, E.; Schwartz, J. K.; Sazanovich, I. V.; Diers, J. R.; Muthukumaran, K.; Taniguchi, M.; Bocian, D. F.; Lindsey, J. S.; Holten, D. *J. Phys. Chem. B* **2003**, *107*, 3443–3454.

(52) Ahrens, M. J.; Sinks, L. E.; Rybtchinski, B.; Liu, W. H.; Jones, B. A.; Giaimo, J. M.; Gusev, A. V.; Goshe, A. J.; Tiede, D. M.; Wasielewski, M. R. *J. Am. Chem. Soc.* **2004**, *126*, 8284–8294.

(53) Li, X. Y.; Sinks, L. E.; Rybtchinski, B.; Wasielewski, M. R. *J. Am. Chem. Soc.* **2004**, *126*, 10810–10811.

(54) Zhang, J.; Hoeben, F. J. M.; Pouderoijen, M. J.; Schenning, A. P. H.; Meijer, E. W.; Schryver, F. C.; De Feyter, S. *Chem. Eur. J.* **2006**, *12*, 9046–9055.

(55) Rybtchinski, B.; Sinks, L. E.; Wasielewski, M. R. *J. Am. Chem. Soc.* **2004**, *126*, 12268–12269.

(56) Ahrens, M. J.; Kelley, R. F.; Dance, Z. E. X.; Wasielewski, M. R. *Phys. Chem. Chem. Phys.* **2007**, *9*, 1469–1478.

(57) Weller, A. *Z. Phys. Chem.* **1982**, *133*, 93–98.

(58) Seidel, C. A. M.; Schulz, A.; Sauer, M. H. M. *J. Phys. Chem.* **1996**, *100*, 5541–5553.

(59) Veldman, D.; Chopin, S. M. A.; Meskers, S. C. J.; Groeneveld, M. M.; Williams, R. M.; Janssen, R. A. J. *J. Phys. Chem. A* **2008**, *112*, 5846–5857.

(60) Lewis, F. D.; Liu, X.; Miller, S. E.; Hayes, R. T.; Wasielewski, M. R. *J. Am. Chem. Soc.* **2002**, *124*, 14020–14026.

(61) Tavernier, H. L.; Fayer, M. D. *J. Phys. Chem. B* **2000**, *104*, 11541–11550.

(62) Kelley, R. F.; Tauber, M. J.; Wasielewski, M. R. *J. Am. Chem. Soc.* **2006**, *128*, 4779–4791.

(63) Lewis, F. D.; Zhang, L.; Kelley, R. F.; McCamant, D.; Wasielewski, M. R. *Tetrahedron* **2007**, *63*, 3457–3464.

(64) Closs, G. L.; Forbes, M. D. E.; Norris, J. R. *J. Phys. Chem.* **1987**, *91*, 3592–3599.

(65) Hore, P. J.; Hunter, D. A.; McKie, C. D.; Hoff, A. J. *Chem. Phys. Lett.* **1987**, *137*, 495–500.

(66) Hasharoni, K.; Levanon, H.; Greenfield, S. R.; Gosztola, D. J.; Svec, W. A.; Wasielewski, M. R. *J. Am. Chem. Soc.* **1996**, *118*, 10228–10235.

(67) Carbonera, D.; DiValentin, M.; Corvaja, C.; Agostini, G.; Giacometti, G.; Liddell, P. A.; Kuciauskas, D.; Moore, A. L.; Moore, T. A.; Gust, D. *J. Am. Chem. Soc.* **1998**, *120*, 4398–4405.

(68) Kobori, Y.; Yamauchi, S.; Akiyama, K.; Tero-Kubota, S.; Imahori, H.; Fukuzumi, S.; Norris, J. R., Jr *Proc. Natl. Acad. Sci. U.S.A.* **2005**, *102*, 10017–10022.

(69) Norris, J. R.; Morris, A. L.; Thurnauer, M. C.; Tang, J. *J. Chem. Phys.* **1990**, *92*, 4239–4249.

(70) Buckley, C. D.; Hunter, D. A.; Hore, P. J.; McLauchlan, K. A. *Chem. Phys. Lett.* **1987**, *135*, 307–312.

(71) Efimova, O.; Hore, P. J *Biophys. J.* **2008**, *94*, 1565–1574.

(72) Gaines, G. L., III; O'Neil, M. P.; Svec, W. A.; Niemczyk, M. P.; Wasielewski, M. R. *J. Am. Chem. Soc.* **1991**, *113*, 719–721.

(73) Huttermann, J.; Voit, K.; Oloff, H.; Kohnlein, W.; Graslund, A.; Rupprecht, A. *Faraday Discuss.* **1984**, 135–149.

(74) Tauber, M. J.; Kelley, R. F.; Giaimo, J. M.; Rybtchinski, B.; Wasielewski, M. R. *J. Am. Chem. Soc.* **2006**, *128*, 1782–1783.

(75) De Kanter, F. J. J.; Kaptein, R.; Van Santen, R. A. *Chem. Phys. Lett.* **1977**, *45*, 575–579.

(76) Anderson, P. W. *Phys. Rev.* **1959**, *115*, 2–13.

(77) Feher, G.; Okamura, M. In *Tunneling Conference*; Chance, B., Devault, D., Frauenfelder, H., Marcus, R. A., Schreiffer, J. R., Sutin, N., Eds.; Academic Press: New York, 1979; pp 729−743.

(78) Nelsen, S. F.; Ismagilov, R. F.; Teki, Y. *J. Am. Chem. Soc.* **1998**, *120*, 2200–2201.

(79) Marcus, R. A. *J. Chem. Phys.* **1965**, *43*, 679–701.

(80) Jortner, J. *J. Chem. Phys.* **1976**, *64*, 4860–4867.

(81) Hasharoni, K.; Levanon, H.; Greenfield, S. R.; Gosztola, D. J.; Svec, W. A.; Wasielewski, M. R. *J. Am. Chem. Soc.* **1995**, *117*, 8055–8056.

(82) Kottis, P.; Lefebvre, R. *J. Chem. Phys.* **1963**, *41*, 379–393.